High-fidelity global optimization of shape design by dimensionality reduction, metamodels and deterministic particle swarm

Xi Chen[ab], Matteo Diez[bc], Manivannan Kandasamy[b], Zhiguo Zhang[a],
Emilio F. Campana[c] & Frederick Stern[b]

[a] School of Naval Architecture and Ocean Engineering, Huazhong
University of Science and Technology, Wuhan, PR China

[b] IIHR-Hydroscience and Engineering, The University of Iowa, Iowa
City, Iowa, USA

[c] CNR-INSEAN, National Research Council–Marine Technology
Research Institute, Rome, Italy
Published online: 20 Mar 2014.

PLEASE SCROLL DOWN FOR ARTICLE

Taylor & Francis
Taylor & Francis Group

High-fidelity global optimization of shape design by dimensionality reduction, metamodels and deterministic particle swarm

Xi Chen[a,b], Matteo Diez[b,c], Manivannan Kandasamy[b], Zhiguo Zhang[a], Emilio F. Campana[c] and Frederick Stern[b*]

[a]*School of Naval Architecture and Ocean Engineering, Huazhong University of Science and Technology, Wuhan, PR China;* [b]*IIHR-Hydroscience and Engineering, The University of Iowa, Iowa City, Iowa, USA;* [c]*CNR-INSEAN, National Research Council–Marine Technology Research Institute, Rome, Italy*

Advances in high-fidelity shape optimization for industrial problems are presented, based on geometric variability assessment and design-space dimensionality reduction by Karhunen–Loève expansion, metamodels and deterministic particle swarm optimization (PSO). Hull-form optimization is performed for resistance reduction of the high-speed Delft catamaran, advancing in calm water at a given speed, and free to sink and trim. Two feasible sets (A and B) are assessed, using different geometric constraints. Dimensionality reduction for 95% confidence is applied to high-dimensional free-form deformation. Metamodels are trained by design of experiments with URANS; multiple deterministic PSOs achieve a resistance reduction of 9.63% for A and 6.89% for B. Deterministic PSO is found to be effective and efficient, as shown by comparison with stochastic PSO. The optimum for A has the best overall performance over a wide range of speed. Compared with earlier optimization, the present studies provide an additional resistance reduction of 6.6% at 1/10 of the computational cost.

List of symbols

A_{ws}	static wetted surface area (m²)
A_{wso}	static wetted surface area of the original model (m²)
C_t	total resistance coefficient $= \frac{R_t}{0.5\rho U^2 A_o}$
C_f	friction resistance coefficient
C_r	residuary resistance coefficient
D	experimental data value
ε_{12}	change between solutions S_1 and S_2
E	comparison error

---

*Corresponding author. Email: frederick-stern@uiowa.edu

f	objective function
Fr	Froude number $= \frac{U}{\sqrt{gL_{pp}}}$
g	acceleration due to gravity $= 9.81$ m/s^2
$\mathbf{g}(\mathbf{x})$	hull geometry
$g_j(\mathbf{x})$	jth inequality constraint
$h_j(\mathbf{x})$	jth equality constraint
λ_k	kth Karhunen–Loève expansion eigenvalue
L_{OA}	length overall (m)
L_{pp}	length between perpendiculars (m)
N_r	number of random particle swarm optimization procedures
N_s	particle swarm size
P	order of convergence
ψ_k	kth principal geometry, provided by Karhunen–Loève expansion
r	grid refinement ratio
R	convergence ratio
R_t	total resistance (N)
S	computational fluid dynamics solution value
U	velocity (m/s)
U_y	uncertainty associated with quantity y
W	ship weight force (N)
x_k	design variables
δ	non-dimensional displacement
ρ	water density at operating temperature (kg/m^3)
σ	non-dimensional sinkage
τ	trim (rad)

1. Introduction

Simulation-based design (SBD) optimization constitutes an essential part of the design process for complex engineering systems. High-fidelity simulations are used with minimization algorithms to identify the best solution to the design problem. Within shape design, simulation tools are integrated with geometry modification and automatic meshing algorithms (Kotinis and Kulkarni 2012). Shape optimization has been widely applied in aerospace, automotive and naval applications, including structural optimization (Papadrakakis, Tsompanakis, and Lagaros 1999), computational fluid dynamics (CFD)-based design (Mohammadi and Pironneau 2004) and fluid–structure interaction (Jakobsson and Amoignon 2007). High-fidelity simulation-based shape design for complex industrial problems remains a demanding process, from theoretical, algorithmic and technological viewpoints.

Potential improvements in shape optimization depend on the dimensionality and geometric variability of the research space. Low-dimension and low-variability spaces are usually easy to explore, but the expected improvement is usually small. High-dimension and high-variability spaces are usually more difficult and expensive to explore but potentially allow for greater improvements. Shape optimization research focused on shape and topology parameterization as critical issues to achieve the desired design variability (Samareh 2001). Geometry can be represented and modified by means of polynomials, splines (Haftka and Grandhi 1986), B-splines (Grigoropoulos and Chalkias 2010), non-uniform rational B-spline (NURBS) and Bezier curves (Campana *et al.* 2006), free-form deformation (FFD) (Peri and Campana 2008), morphing approaches (Kandasamy *et al.*

2013), basis vector methods, domain element and discrete approaches (Samareh 2001). In most studies, the trade-off between geometric variability and space dimensionality is not addressed or is only qualitatively assessed.

Karhunen–Loève expansion (KLE) was used for representing distributed geometric uncertainties and building reduced-order spatial models for uncertainty quantification by Borzì *et al.* (2010) and Schillings, Schmidt, and Schulz (2011). Diez, Campana, and Stern (2012) used KLE to assess the geometric variability of the optimization research space and build a reduced-dimensionality global model. Reduced-dimensionality models based on KLE were used by Diez, Campana, and Stern (2013) and He *et al.* (2013) for design-related geometric uncertainty quantification. Raghavan *et al.* (2013) make use of principal components analysis for building a reduced-order local model for shape representation. Applications and theory of dimensionality reduction for high-fidelity shape optimization remain limited.

To reduce the computational cost, SBD is often performed by surrogate models (Won and Ray 2005). Recent research in metamodelling moved from static to dynamic approaches (adaptive sampling and auto-tuning) (Zhao, Choi, and Lee 2011) and from single models to ensemble of surrogates (Goel *et al.* 2007). The reliability of metamodels during optimization remains a critical issue, especially when global optimization is performed.

Derivative-free global optimization procedures, such as particle swarm optimization (PSO) (Kennedy and Eberhart 1995), are usually preferred to derivative-based local approaches when objectives are noisy, derivatives are unknown and the existence of multiple local optima cannot be excluded. For ship hydrodynamics applications, it has been shown that derivative-free global algorithms are more effective than local methods (Campana *et al.* 2009). When global techniques are used with high-fidelity solvers, the optimization process is computationally expensive and its efficiency remains an algorithmic and technological challenge.

Traditionally, in ship design the hull shape is evaluated by towing tank experiments aimed at total resistance at fixed speeds in calm water. The model is free to achieve its dynamic equilibrium, defined by the sinkage and the trim angle. SBD using high-fidelity CFD is replacing the build-and-test approach, providing opportunities for improved analyses and innovative/optimized designs. SBD is demonstrating capabilities for complex applications including the topic of the present research, *i.e.* the high-speed Delft catamaran (DC), a concept ship used as a benchmark for numerical and experimental studies. SBD for the DC is given by Kandasamy *et al.* (2013), where the hull form and waterjet system were optimized using global evolutionary algorithms with a morphing technique for the hull modification, based on six initial designs and allowing for a 3% reduction in calm-water resistance. Diez *et al.* (2012) showed that the morphing approach used was too stiff, not allowing for large design variability. Some of the initial designs were found to be linearly dependent, thus providing a degenerated research space with a number of design variables greater than the space dimension. Identification of the optimal shapes required a large simulations budget.

The objective of the present research is the development and application of a methodology for effective, efficient and reliable high-fidelity global optimization for shape design, based on design-space dimensionality reduction by KLE, multiple metamodels using global and local design of experiments (DoE), and multiple global minimization procedures.

KLE is applied to reduce the dimensionality of an FFD design space, retaining 95% of the original geometric variance. Deterministic PSO (Campana *et al.* 2009) is used with several coefficient sets. To confirm the effectiveness and efficiency of deterministic PSO, this is compared with statistically converged results from stochastic PSO, for one of the problems solved. Multiple approximation models are used, coupled with a DoE method, and trained by URANS. The application is the shape optimization of the DC bare hull. The design objective is to minimize the calm-water resistance at fixed speed. Two feasible sets are investigated, based on different geometric constraints.

2. Simulation-based design problem formulation

The DC parent hull is shown in Figure 1 and details are given in Kandasamy et al. (2013). The model is free to sink and trim. Herein, a full-scale length equal to 100 m and a design speed equal to 29 kt is assumed, corresponding to Froude number (Fr) equal to 0.5, and dimensional speed equal to 2.98 m/s for a 3.627 m towing tank model. Reduction of power required, $P = R_t U$, is taken as the optimization objective (U is the ship speed and R_t the total resistance). Since U is equal to the design speed, the optimization objective reduces to R_t.

Geometry modifications have to fit in a box, defined by maximum overall length, beam and draught. The ship displacement is considered fixed (within a 1% tolerance). A similar approach was used by Tahara et al. (2011) for high-speed multihull optimization, and Grigoropoulos and Chalkias (2010) for monohulls. As a significant design parameter, the length between perpendiculars, L_{pp}, is often considered to be fixed, as shown in Kandasamy et al. (2013). To compare the present research with earlier work, two constraints sets are used and shown in Table 1. The first (referred to as problem A) includes the overall dimension bounds; the second (referred to as problem B) includes the overall dimension bounds and, in addition, constant length between perpendiculars.
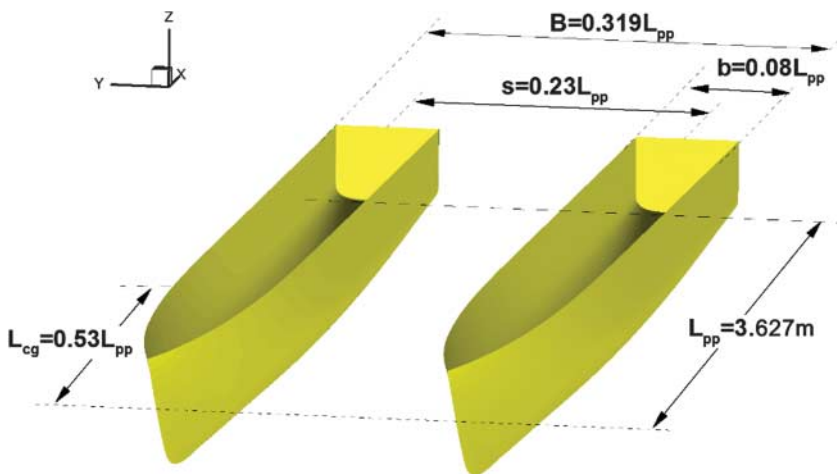
Figure 1.   Main dimensions for Delft catamaran 372 model.

Table 1.   Geometric constraints sets and optimization problems.

Problem	Geometric constraints	Value[a]	No. of design variables	Objective	Simulations budget
A	Max. overall length, L_{OA}	100	4	R_t/W evaluated at design speed	120
	Max. beam, B	100			
	Max. draught, T	100			
	Max. displacement variation, $|\Delta\delta|$	1			
B	Same as problem A, with in addition: constant length between perpendiculars, L_{pp}	100	6		180

Note: [a]Values refer to % of original hull.

The design problem is formulated as a constrained single-objective minimization problem:

$$
\begin{aligned}
&\text{Minimize} f(\mathbf{x}) \\
&\text{subject to } l_k \leq x_k \leq u_k, \quad k = 1, \ldots, n \\
&\text{and to } g_j(\mathbf{x}) \leq 0, \quad j = 1, \ldots, G \\
&\text{and to } h_j(\mathbf{x}) = 0, \quad j = 1, \ldots, H
\end{aligned}
\tag{1}
$$

where $\mathbf{x}$ is the design variables vector $\{x_k\}_{k=1}^n$, with bounds l_k, and u_k; x_k provide global hull-geometry modifications, based on FFD and KLE as per Section 3.1. These modify simultaneously ship length, demi-hull beam, draught, waterline design, and associated centre of buoyancy and block coefficient. Functions in Equation (1) are:

$$
f(\mathbf{x}) = \frac{R_t(\mathbf{x})}{W(\mathbf{x})} \quad g_1(\mathbf{x}) = \frac{L_{OA}(\mathbf{x})}{L_{OA,ori}} - 1 \quad g_2(\mathbf{x}) = \frac{B(\mathbf{x})}{B_{ori}} - 1
$$

$$
g_3(\mathbf{x}) = \frac{T(\mathbf{x})}{T_{ori}} - 1 \quad g_4(\mathbf{x}) = \left| \frac{\delta(\mathbf{x}) - \delta_{ori}}{\delta_{ori}} \right| - 10^{-2}
\tag{2}
$$

with the additional constraint for problem B,

$$
h_1(\mathbf{x}) = \frac{L_{pp}(\mathbf{x})}{L_{pp,ori}} - 1
\tag{3}
$$

where W is the ship weight force, L_{OA} is the overall length, B is the beam, T is the draught, and δ is the ship (non-dimensional) displacement. Subscript *ori* indicates parent hull values.

3. Simulation-based design framework

The SBD framework includes geometry modifications based on FFD and dimensionality reduction by KLE, multiple global metamodels and minimization procedures based on DoE using URANS and PSO, as shown in Figure 2. The procedure follows two macro-iterations; the first includes initial global DoE, surrogate analysis and optimization, whereas the second encompasses a refinement of the training set.

3.1. *Geometry modifications by free-form deformation and Karhunen–Loève expansion*

KLE, also known as proper orthogonal decomposition and equivalent (under certain conditions) to principal components analysis, provides a breakdown of the geometric variability spanned within the design space and is used for dimensionality reduction, based on 95% confidence (Diez *et al.* 2012). Before optimization, the shape design problem is considered as a problem affected by epistemic uncertainty: the optimal solution in considered unknown, with uniform probability of occurrence in the design space. This is sampled randomly using a number of S geometries, $\{\mathbf{g}_j\}_{j=1}^S$. Random items are given by arbitrary geometry deformation techniques. FFD is used herein since it allows for high design flexibility and is independent of grid topology (Peri and Campana 2008).
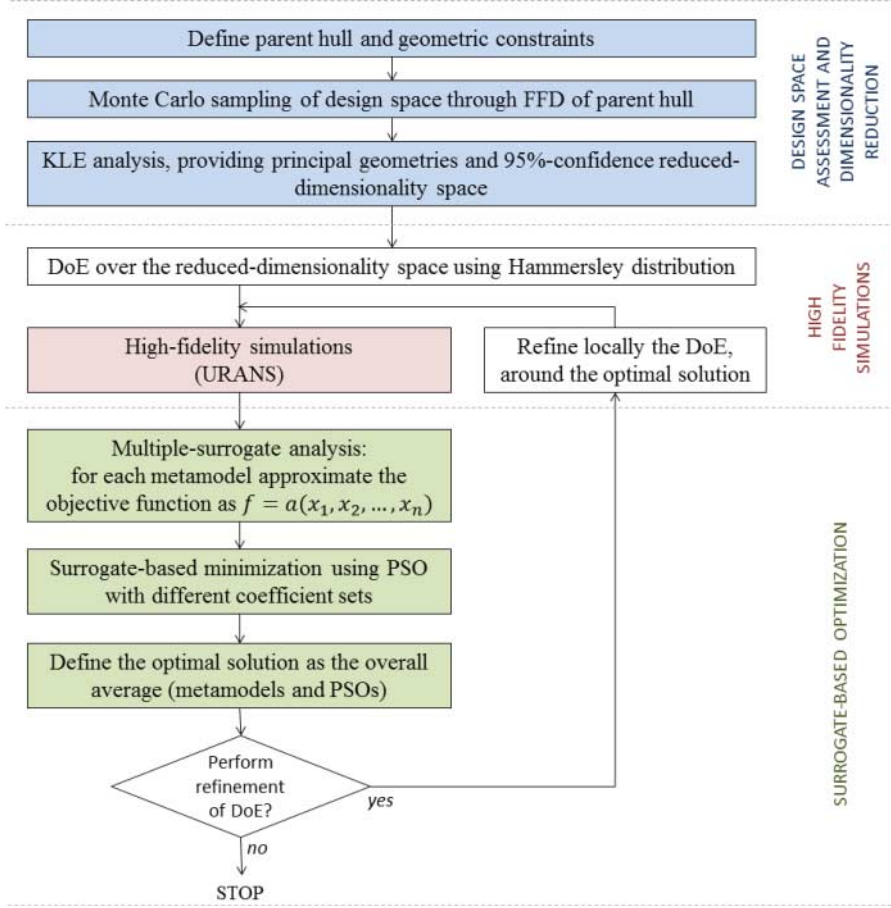
Figure 2.   Simulation-based design procedure. FFD = free-form deformation; KLE = Karhunen–Loève expansion; DoE = design of experiments; PSO = particle swarm optimization.

The mean geometry is defined as

$$\bar{\mathbf{g}} = \frac{1}{S} \sum_{j=1}^{S} \mathbf{g}_j \tag{4}$$

The principal directions, $\mathbf{z}_k$, of the research space defined by the linear expansion (formally the KLE of the geometry modifications space)

$$\mathbf{g} = \bar{\mathbf{g}} + \sum_{k=1}^{K} \alpha_k \mathbf{z}_k \tag{5}$$

are solutions of the eigenproblem

$$\mathbf{R}\mathbf{z}_k = \lambda_k \mathbf{z}_k \tag{6}$$

where $\mathbf{R} = (\mathbf{G}\mathbf{G}^T)/S$, with $\mathbf{G} = [\mathbf{g}_1 - \bar{\mathbf{g}} \ldots \mathbf{g}_S - \bar{\mathbf{g}}]$. $K = 3N_G$ is the actual dimension of the space, with N_G number of grid nodes (three-dimensional case). The eigenvalues λ_k represent the geometric variance associated with the corresponding eigenvector $\mathbf{z}_k$ and are used to assess the total geometric variance and build a reduced-dimensionality space, based on 95% confidence

as:

$$\mathbf{g}(\mathbf{x}) = \left(1 - \sum_{k=1}^{n} x_k\right)\bar{\mathbf{g}} + \sum_{k=1}^{n} x_k \psi_k \tag{7}$$

where $\psi_k = \bar{\mathbf{g}} + \sup\{\mathbf{G}^T \mathbf{z}_k\}\mathbf{z}_k$, $-1 \leq x_k \leq 1$, and n is chosen such that

$$\sum_{k=1}^{n} \lambda_k \geq 0.95 \sum_{k=1}^{K} \lambda_k \tag{8}$$

with

$$\sum_{k=1}^{K} \lambda_k = \frac{1}{S} \sum_{j=1}^{S} (\mathbf{g}_j - \bar{\mathbf{g}})^2 = \text{Var}(\mathbf{g}) \tag{9}$$

defining the total geometric variance of the space.

Equations (4)–(9) represent the framework for research space dimensionality reduction and can be applied to arbitrary geometry modification techniques, taking as input a random set of shape designs and providing as output the principal directions of the design space (eigenvectors) with the associated geometric variance (eigenvalues). New designs are generated as per Equation (7), by linear combination of principal geometries. According to KLE theory, no greater geometric variance can be retained by any other linear expansion of order n. Using Equations (4)–(9), research spaces can be reduced in dimensionality before optimization, with a significant increase in SBD efficiency.

3.2. *Global minimization algorithm: deterministic particle swarm optimization*

PSO iteration is given by

$$\mathbf{v}_j^i = \chi[w\mathbf{v}_j^{i-1} + r_1 c_1(\mathbf{p}_j - \mathbf{x}_j^{i-1}) + r_2 c_2(\mathbf{g} - \mathbf{x}_j^{i-1})] \tag{10}$$

$$\mathbf{x}_j^i = \mathbf{x}_j^{i-1} + \mathbf{v}_j^i \tag{11}$$

for $j = 1,\ldots,N_s$, where N_s is the swarm size; $\mathbf{x}_j^i$ is the position of the jth particle at the ith iteration, $\mathbf{p}_j$ is the best position ever visited by the jth particle (personal optimum), and $\mathbf{g}$ is the overall best position ever visited by all the particles (global or social optimum); χ, w, c_1 and c_2 are coefficients or weights controlling damping, inertia and personal/social behaviour of the swarm; r_1 and r_2 are random coefficients (uniformly distributed from 0 to 1) used by Kennedy and Eberhart (1995). When deterministic PSO is used, $r_1 = r_2 = 1$. Three sets of deterministic coefficients are used herein, taken from Eberhart and Shi (2000), Shi and Eberhart (1998), and Peri and Tinti (2012), as summarized in Table 2, which also includes random implementation. The latter is assessed focusing on expected value (*EV*) and standard deviation (*SD*) of minimum $\hat{f}$

$$EV(\hat{f}) = \frac{1}{N_r} \sum_{i=1}^{N_r} \hat{f}_i \quad SD(\hat{f}) = \sqrt{\frac{1}{N_r} \sum_{i=1}^{N_r} \left[\hat{f}_i - EV(\hat{f})\right]^2} \tag{12}$$

along with their convergence ratio and absolute per cent solution change (Mousaviraad *et al.* 2013)

$$R_k = \frac{Y_k - Y_{k-1}}{Y_{k-1} - Y_{k-2}} \quad N_{r,k} = N_{r,0} 2^{k-1} \tag{13}$$

where k indicates the convergence iteration and Y stands for *EV* or *SD*. Iterations are defined by a sample size equal to $N_{r,k} = N_{r,0} 2^{k-1}$, where $N_{r,0}$ indicates initial value. $|R|$ is required to be less than 1, with $\varepsilon \leq 1\%$.

Table 2.   Initial speed and coefficient sets used for particle swarm optimization (PSO).

PSO coefficient set #	Initial speed	Coefficients, as per Equation (10)				
		c_1	c_2	w	χ	Ref.
1	Null	1.494	1.494	0.729	1.000	Eberhart and Shi (2000)
2		1.200	1.200	0.900	1.000	Shi and Eberhart (1998)
3		2.042	1.150	0.720	1.047	Peri and Tinti (2012)
4	Hammersley, Equation (15)	1.494	1.494	0.729	1.000	Eberhart and Shi (2000)
5		1.200	1.200	0.900	1.000	Shi and Eberhart (1998)
6		2.042	1.150	0.720	1.047	Peri and Tinti (2012)
Random		2.000	2.000	1.000	1.000	Kennedy and Eberhart (1995)

During swarm optimization, box and functional inequality constraints are treated by a linear penalty function of the type:

$$\phi(\mathbf{x}) = \begin{cases} \dfrac{1}{\eta} g(\mathbf{x}), & g(\mathbf{x}) > 0 \\ 0, & \text{otherwise} \end{cases} \quad (14)$$

with $\eta = 0.01$. $\mathbf{p}_j$ and $\mathbf{g}$ in Equation (10) are based on $\hat{f}(\mathbf{x}) = f(\mathbf{x}) + \phi(\mathbf{x})$. Equality constraints are automatically satisfied by the geometry modification.

The swarm dimension N_s is set to 20 n, where n is the design space dimension. The initial swarm position, $\mathbf{x}_j^0$, is defined using a Hammersley distribution (Wong, Luk, and Heng 1997) over the design space of Equation (7). The initial speed, $\mathbf{v}_j^0$, is considered null or equal to

$$\mathbf{v}_j^0 = \frac{2}{\sqrt{n}} \left[\mathbf{x}_j^0 - \frac{(\mathbf{l} + \mathbf{u})}{2} \right] \quad (15)$$

where $\mathbf{l}$ and $\mathbf{u}$ are lower and upper bound vectors, as per Equation (1). The maximum number of PSO iterations is set to 100. The resulting maximum number of function evaluations is 2000 n per PSO procedure. Combining different deterministic coefficient sets with initial speed assumptions results in six separate PSO procedures (Table 2).

3.3.   *Design of experiments and metamodels*

All metamodels are trained using an initial DoE, which follows a Hammersley distribution. The training set size is set to 20 n. The following metamodels are used: stochastic ensemble of radial basis functions network (SE-RBFN) with (1) power law kernel and (2) multiquadric kernel; ordinary kriging (OKG) with (3) exponential covariance function and (4) linear covariance function; least-square support vector machine (LS-SVM) with (5) multiquadric kernel and (6) inverse multiquadric kernel; and polyharmonic spline (PHS) of (7) first order and (8) second order. SE-RBFN is based on Volpi (2013), OKG is taken from Peri (2009), and LS-SVM and PHS are based on Suykens *et al.* (2002) and Wahba (1990), respectively. Metamodel parameters are taken from Diez *et al.* (2013) and He *et al.* (2013), where surrogate model studies were conducted and discussed for the DC advancing in calm water and waves, including variable speed, wave parameters and geometry. Deterministic PSO procedures in Table 2 are performed for each metamodel, resulting in 48 optimizations. The optimization result is given as the average among all optimal solutions.
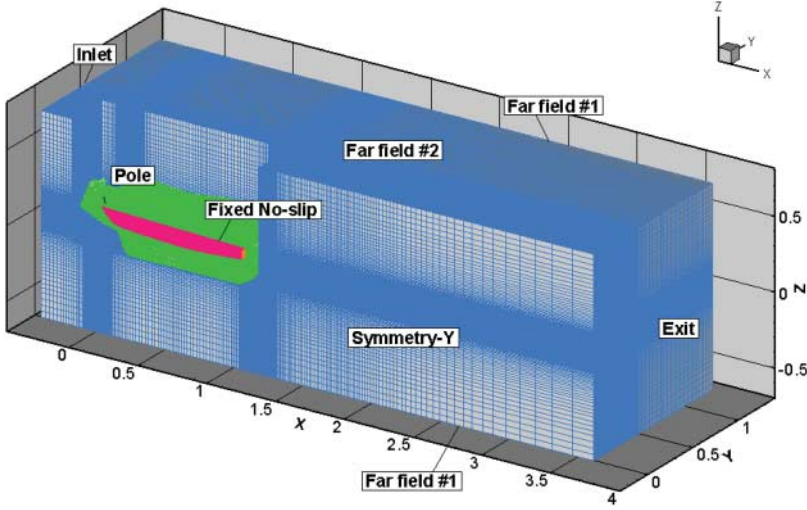
Figure 3. Grid used in the current study.

3.4. *Computational fluid dynamics method, simulation conditions and computational domain*

CFDShip-IOWA, a URANS code for ship hydrodynamics, is used as a flow solver (Huang, Carrica, and Stern 2008). The waterjet (WJ) propulsion is considered through a simplified model. This incorporates the effects of the WJ-induced vertical forces and pitching moments, without requiring detailed simulations of duct flow (Kandasamy *et al.* 2010). Simulations are conducted in calm water at Fr = 0.5 and Reynolds number Re = 1.019×10^7 (based on parent hull L_{pp}). Grids are generated in a non-dimensional coordinate system, normalized by parent hull L_{pp}. The longitudinal axis of the ship is placed on the *x*-axis with the bow at $x = 0$, stern at $x = 1$ and waterline at $z = 0$. The computational domain extends within $-0.4 \leq x \leq 3.6$, $0 \leq y \leq 1.3$, $-0.7 \leq z \leq 0.66$ (Figure 3).

3.5. *Validation and verification method*

To ensure the significance of the optimization, simulations have to be validated and the improvement achieved has to be larger than numerical uncertainties. Following the factor of safety method (Xing and Stern 2010), verification estimates the numerical uncertainty (U_{SN}) as $U_{SN} = \sqrt{U_I^2 + U_G^2}$, where U_I is the iterations uncertainty, and grid uncertainty U_G is estimated from grid studies. Validation uncertainty (U_V) is assessed using experimental data (D) with uncertainty U_D and numerical uncertainty U_{SN} as $U_V = \sqrt{U_D^2 + U_{SN}^2}$. If $|E| = |D - S| < U_V$, validation is achieved at the U_V interval.

The optimized design is numerically verified by the condition (Campana *et al.* 2006):

$$|\Delta S| > U_{\Delta S} = \sqrt{U_{SN,ori}^2 + U_{SN,opt}^2} \tag{16}$$

where ΔS is the improvement achieved by optimization, $U_{SN,ori}$ is the numerical uncertainty of the parent hull, and $U_{SN,opt}$ is that of the optimized design.

Table 3.   Verification and validation without waterjet (WJ) model.

Bare hull	Triplet	r	Verification							Validation			
			R	P	U_I	U_o	U_I/ε_{12}	U_I/U_o	U_{SN}	U_D	U_{SN}/U_D	U_V	E
C_t	1,2,3	$\sqrt{2}$	0.622	0.686	0.083	3.986	0.064	2.093	3.987	0.210	18.986	3.954	−0.978
	2,3,4		0.180	2.472	0.094	11.976	0.045	0.786	11.977		57.032	11.708	−2.264
C_f	1,2,3		1.637	MD	0.097	–	0.145	–	–	–	–	–	–
	2,3,4		1.494	MD	0.071	–	0.173	–	–		–	–	–
C_r	1,2,3		0.521	0.940	0.093	3.297	0.051	2.821	3.298	–	–	–	–
	2,3,4		0.166	2.592	0.123	19.737	0.034	0.622	19.737		–	–	–
σ	1,2,3		0.551	0.859	0.074	1.644	0.096	4.524	1.646	1.310	1.256	2.158	4.240
	2,3,4		0.074	3.750	0.001	5.334	0.001	0.017	5.334		4.072	5.670	3.428
τ	1,2,3		0.531	0.913	0.008	4.231	0.004	0.185	4.231	2.910	1.454	5.103	−0.922
	2,3,4		0.165	2.603	0.001	23.599	0.000	0.003	23.599		8.109	23.273	−2.153

Note: U_I, U_G and U_{SN} are $\%S_1$; S_1 is the solution of finest grid in each triplet; U_D, U_V and E are $\%D$.

Table 4.   Verification with waterjet (WJ) model.

Bare hull with WJ effect	Triplet	R	Verification						
			R	P	U_I	U_G	U_I/ε_{12}	$U_I\%U_G$	U_{SN}
C_t	1,2,3	$\sqrt{2}$	0.602	0.732	0.102	3.713	0.076	2.751	3.714
	2,3,4		0.172	2.537	0.141	12.557	0.063	1.122	12.558
C_f	1,2,3		1.657	MD	0.099	–	0.132	–	–
	2,3,4		1.221	MD	0.095	–	0.210	–	–
C_r	1,2,3		0.494	1.018	0.127	3.410	0.069	3.729	3.412
	2,3,4		0.159	2.657	0.190	20.507	0.050	0.927	20.508
σ	1,2,3		0.721	0.473	0.001	4.481	0.001	0.012	4.481
	2,3,4		0.069	3.859	0.001	4.265	0.000	0.012	4.265
τ	1,2,3		0.499	1.003	0.000	2.775	0.000	0.014	2.775
	2,3,4		0.167	2.580	0.000	19.096	0.000	0.002	19.096

Note: U_I, U_G and U_{SN} are $\%S_1$, where S_1 is the solution of the finest grid in each triplet.

4.   Results

4.1.   *Validation and verification of original hull*

Verification is assessed for total, frictional and residuary resistance coefficients, C_t, C_f and C_r; non-dimensional sinkage, $\sigma = \Delta z_G/L_{pp}$; and trim, τ. Four grids, G1–4, are used with size ranging from 1.7 to 37.3 m and associated $y+ < 1$, enabling two triplets with refinement ratio equal to $\sqrt{2}$.

Table 3 presents verification and validation studies for bare hull without WJ effects, to validate the simulations against available experimental data, provided by CNR-INSEAN and presented in Kandasamy *et al.* (2013). U_I is small compared to S_1, ε_{12} and U_G. Monotonic convergence is achieved for all variables and triplets except C_f. $P < 1$ for a fine triplet, whereas it is > 2 using a coarse triplet. Triplet (1,2,3) gives average U_G for C_t, C_r, σ and τ equal to 3.29% on G1; triplet (2,3,4) gives average U_G equal to 12.66% on G2. Average validation error for C_t, σ and τ by the finest grid (G1) is fairly small and equal to 2.05%D. Average U_D is small and equal to 1.48%D; results are validated at an average interval of 3.74%D. With increasing grid size, error decreases for resistance and trim, whereas it increases for sinkage. Table 4 shows verification results using a simplified WJ model. Trend is similar to that in Table 3: U_I is small compared to S_1, ε_{12} and U_G; monotonic convergence is achieved for all variables and triplets except C_f. $P < 2$ using a fine triplet, whereas it is > 2 using a coarse triplet. Average U_G for triplet (1,2,3) and C_t, C_r, σ and τ is reasonable and equal to 3.59% on G1; triplet (2,3,4) gives average U_G equal to 14.11% on G2.
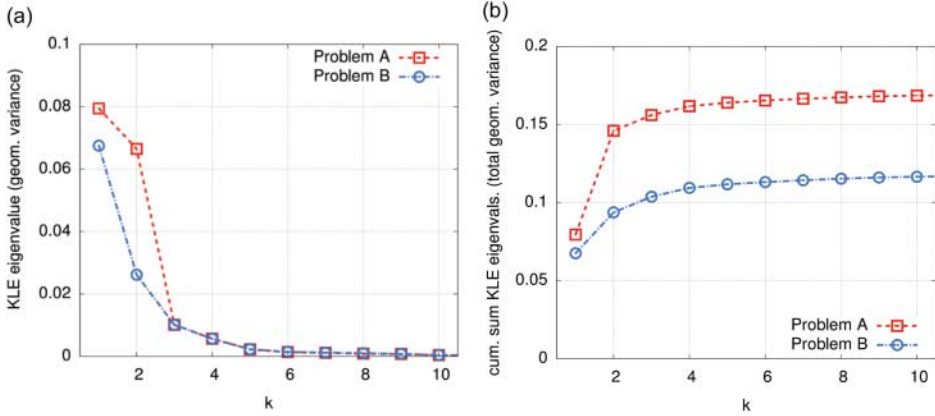
Figure 4. Geometric variability breakdown: (a) Karhunen–Loève expansion (KLE) eigenvalues and (b) their cumulative sum.

4.2. *Karhunen–Loève expansion and preliminary sensitivity analysis along eigenvectors*

Equations (4)–(7) are applied to a 20-dimensional FFD, using $S = 10,000$ random geometries for feasible sets A and B. FFD parameters control the x, y and z displacement of control points of a $9 \times 5 \times 5$ grid, embedding the catamaran hull. Random designs are produced assuming a uniform distribution of the FFD parameters. Herein, the mean geometry, Equation (4), corresponds to the original shape. The computational grid for KLE of body-surface modifications has a size of 60×30 nodes. Node distance stretches by a factor of 0.9 from deck to bottom, to give more emphasis to submerged nodes. The eigenproblem, Equation (6), has a size of 5400×5400. The eigenvalues are shown in Figure 4, along with the total geometric variance retained by the reduced-dimensionality model. Feasible set A has greater geometric variance than B. Analysis of eigenvalues as per Equation (8) and Figure 4(b) reveals that four principal geometries ψ_k, Equation (7), are necessary for 95% total geometric variance of feasible set A, whereas six geometries are required for B. Figure 5 shows the principal geometries for sets A and B.

Effects of geometric variations along the principal directions are investigated by preliminary sensitivity analysis. Geometries are defined as:

$$\mathbf{g}(x_k) = (1 - x_k)\mathbf{g}_o + x_k\psi_k \tag{17}$$

where $\mathbf{g}_0$ is the original geometry and x_k are the design variables, bounded by $-1 \le x_k \le 1$; five steps are used for each x_k, $k = 1 \ldots, n$.

$\Delta[R_t/W]\%$ is presented in Figure 6, using G2. Changes in $\Delta[R_t/W]$ are found to be significant in each direction. First principal geometries reveal a reduction in resistance of 7% and 5% for A and B, respectively. Sensitivity analysis is also performed using coarser grids G3 and G4. The average error of G3 versus G2 equals 0.61% for problem A and 0.59% for problem B. Average errors for G4 equal 2.70% and 2.31% for A and B, respectively. Pearson's correlation coefficient using G2 and G3 is nearly 1 for both problems, whereas using G2 and G4 gives a correlation equal to 0.82 and 0.81 for A and B, respectively. Accordingly, G3 is deemed appropriate for simulations during optimization.

4.3. *Optimization results*

4.3.1. *Surrogate-based optimization by global design of experiments*

Design optimization is performed over a global window, with box constraints defined by $-1 \le x_k \le 1$, where x_k define the hull shape as per Equation (7). Training set size is set to
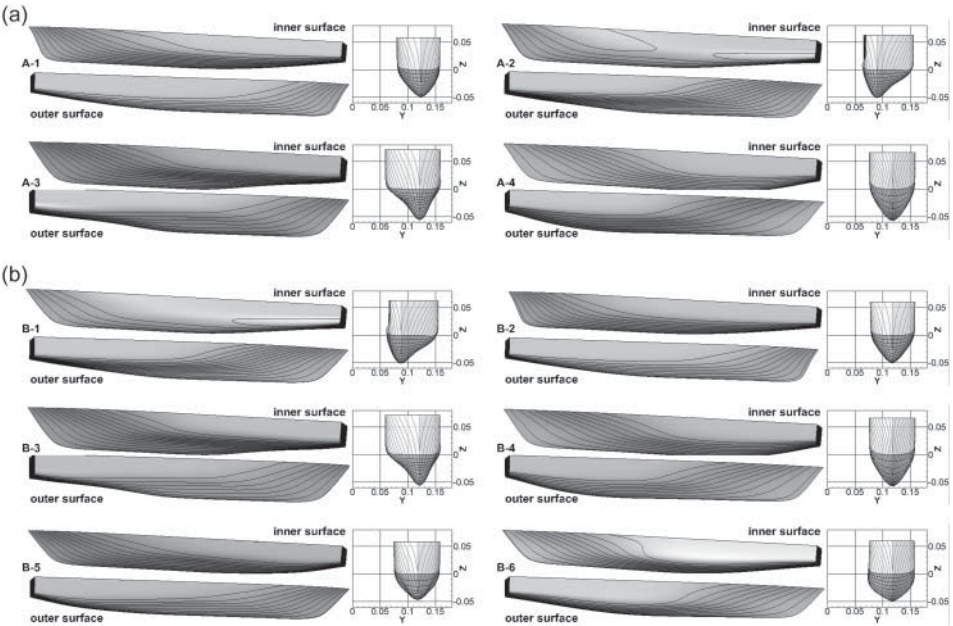
Figure 5.   Principal geometries given by Karhunen–Loève expansion (KLE): (a) problem A and (b) problem B.
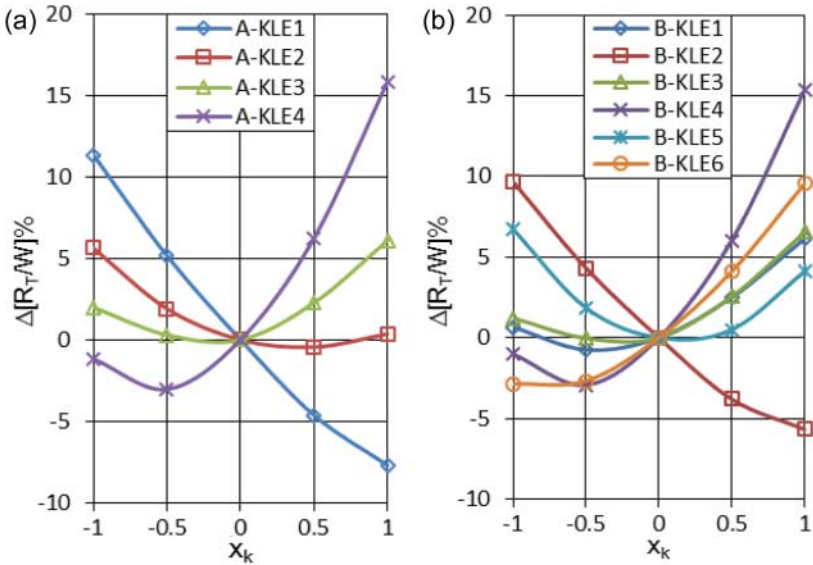

Figure 6. $\Delta[R_t/W]\%$ along principal directions using G2: (a) problem A and (b) problem B. KLE = Karhunen–Loève expansion

80 for problem A and 120 for problem B. All metamodels and PSO combinations give close results. The average solution and standard deviation of the design variables, for different meta-models and deterministic PSO procedures, are shown in Table 5 and Figure 7 for problems A and B, respectively. Standard deviations are reasonable ($\leq 1.6\%$ for problem A and $\leq 15.1\%$ for problem B, compared with the variables range). The average value is taken as the optimum for

Table 5. Deterministic particle swarm optimization results.

Problem	DoE	Average						St. deviation (% of variable range)						Predicted obj. reduction (%)	
		x_1	x_2	x_3	x_4	x_5	x_6	x_1	x_2	x_3	x_4	x_5	x_6	Ave.	St. dev.
A	glob.	0.9609	0.1393	−0.5396	−0.3598			1.60	0.48	3.31	0.29			−8.40	0.24
	ref.	1.1505	0.1646	−0.5850	−0.3124			0.22	0.46	0.67	0.53			−9.92	0.06
B	glob.	0.0982	0.7560	−0.3711	−0.3203	0.1784	−0.0087	0.12	10.2	15.1	6.60	9.62	11.3	−6.05	0.41
	ref.	−0.0177	0.8941	−0.6642	−0.3503	0.1906	3.0393	0.04	0.17	0.07	0.09	0.10	0.08	−6.85	0.02

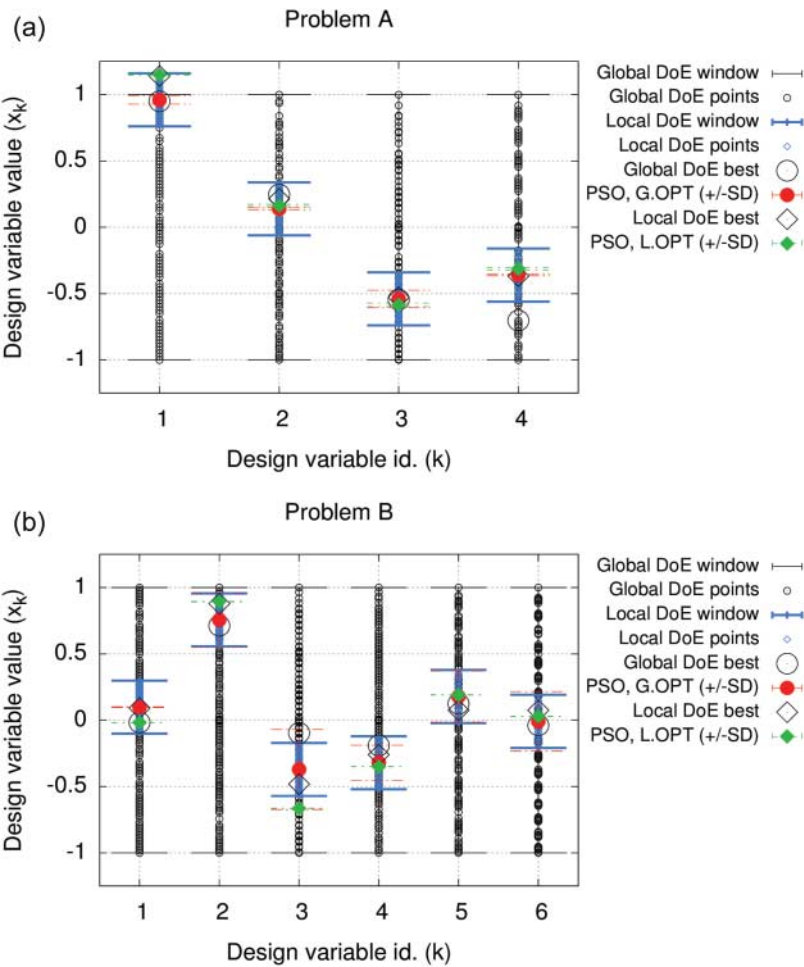Note: DoE = design of experiments.

Figure 7. Particle swarm optimization (PSO) optimal designs: summary of (a) problem A and (b) problem B.

the current macro-iteration, namely G.OPT-A and G.OPT-B, for A and B, respectively. Optimal solutions G.OPT-A and G.OPT-B are verified with URANS and the results are shown in Table 6, giving 9.02% and 6.07% total resistance (over weight) reduction for A and B, respectively.

Table 6. Computational fluid dynamics results for optimal designs from optimization based on global design of experiments.

Optimum	Design variables	L_{PP}		y_{max}		$\delta \times 10^2$		$\sigma \times 10^2$		$\tau \times 10^2$		$R/W \times 10^2$	
		S	$\Delta\%S_0$	S	$\Delta\%S_0$	S	$\Delta\%S_0$	S	$\Delta\%S_0$	S	$\Delta\%S_0$	S	$\Delta\%S_0$
G.OPT-A	(0.9609, 0.1393, −0.5396, −0.3598)	1.0179	1.79	0.1564	−0.173	1.617	−0.010	4.190	−1.334	3.263	−17.991	5.265	−9.020
G.OPT-B	(0.0982, 0.7560, −0.3711, −0.3204, 0.1784, −0.0087)	1	0	0.1566	−0.086	1.615	−0.138	4.241	−0.133	3.452	−13.241	5.436	−6.065

Note: S = URANS solution of optimal geometry; S_0 = URANS solution of original geometry; Δ = URANS solution difference between optimal and original geometries.
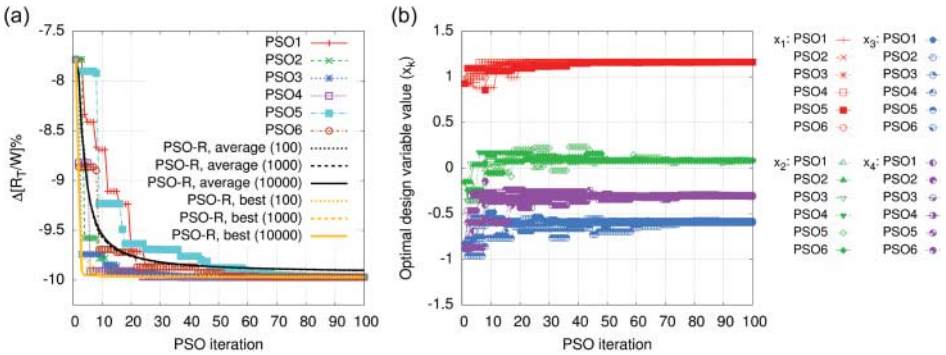

Figure 8. Particle swarm optimization (PSO) by local refinement of design of experiments: (a) optimization objective and (b) optimal design variables value *vs* iterations [problem A with stochastic ensemble of radial basis functions network (SE-RBFN)].

4.3.2. *Surrogate-based optimization by local refinement of design of experiments*

A local refinement is performed, over the region enclosing G.OPT-A and G.OPT-B. A local window is defined such as $-0.2 \leq x_k - x_{k,opt} \leq 0.2$, where $x_{k,opt}$ represents optimal values from the first macro-iteration. A local DoE is used, with additional 40 points for problem A and 60 for B. Accordingly, in local windows the point density increases by a factor of 2.5. Optimization is performed over the design space defined by the Boolean union of global and local windows. Figures 8 and 9 show the PSO convergence for problems A and B, respectively, using the SE-RBFN model and multiple deterministic coefficient sets, as per Table 2. Deterministic PSO procedures have different dynamics, while converging to very similar solutions. Figure 10 shows the statistical convergence of stochastic PSO for problem A, in terms of expected value and lower bound of minimum (a) and associated standard deviation (b), versus the sample size. Convergence is noisy and 10,000 optimizations are required to achieve statistically convergent results, as per Section 3.2. The best solution is achieved after 130 optimizations and approximately equals the deterministic optimum. Specifically, the best random solution is found to be 0.2E-3% greater than the deterministic solution. Convergent results reveal a difference of 0.07% between the minimum expected value and lower bound, whereas the standard deviation is 0.05%. Figure 10(c) presents the histogram analysis of the minimum provided by 10,000 stochastic PSOs, showing that the distribution's lower bound approximately coincides with the deterministic minimum. Figure 8(a) shows average and best global minimum versus the number of swarm iterations, considering 100, 1000 and 10,000 random optimizations, confirming that deterministic and stochastic PSOs converge to the same result. Accordingly, deterministic PSO is extended to other metamodels since it is more efficient. All metamodels and deterministic PSO combinations give close results.
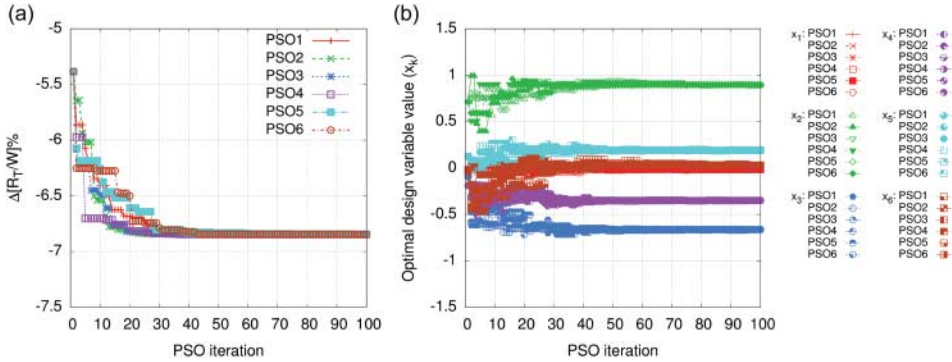
Figure 9. Particle swarm optimization (PSO) by local refinement of design of experiments: (a) optimization objective and (b) optimal design variables value *vs* iterations [problem B with stochastic ensemble of radial basis functions network (SE-RBFN)].
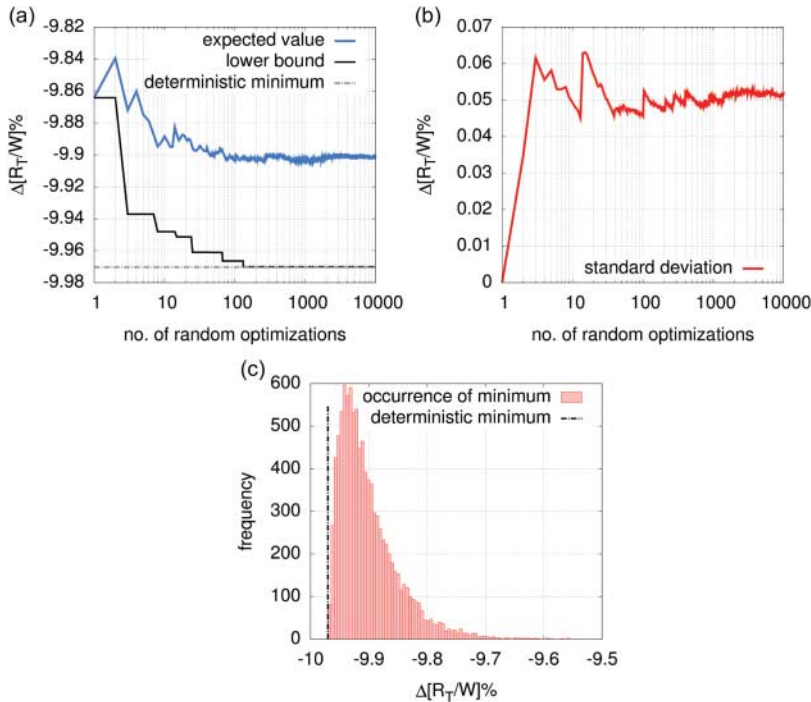

Figure 10. Statistical analysis of random particle swarm optimization [problem A with stochastic ensemble of radial basis functions network (SE-RBFN)]: (a) convergence of expected value and lower bound and (b) standard deviation of optimum; (c) histogram analysis of optimum using 10,000 optimizations.

The average solution and standard deviation of the design variables are shown in Table 5 and Figure 7 for problems A and B, respectively. Standard deviations are very small ($\leq 0.67\%$ for problem A and $\leq 0.17\%$ for problem B), showing beneficial effects of DoE refinement. Average solutions give the final optimal shapes, namely L.OPT-A and L.OPT-B for A and B, respectively.

Figure 11 shows the overall convergence of the SBD optimization, where G.best and L.best indicate the best solutions among global and local DoE points, respectively. The procedure is found to be convergent, revealing a monotonic descent towards the optimal shapes.
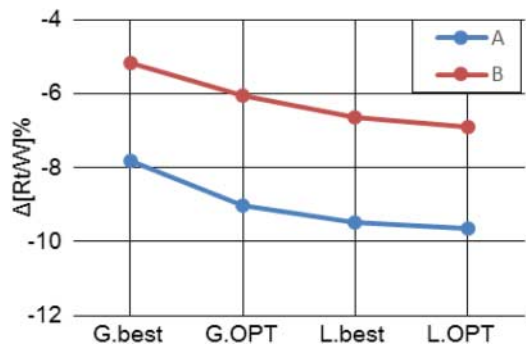
Figure 11.   Simulation-based design optimization convergence.

Table 7.   Computational fluid dynamics results for optimal designs from optimization based on local refinement.

		L_{PP}		y_{max}		$\delta \times 10^2$		$\sigma \times 10^2$		$\tau \times 10^2$		$R/W \times 10^2$	
Optimum	Design variables	S	$\Delta\%S_0$	S	$\Delta\%S_0$	S	$\Delta\%S_0$	S	$\Delta\%S_0$	S	$\Delta\%S_0$	S	$\Delta\%S_0$
L.OPT-A	(1.1505, 0.1646, −0.5850, −0.3124)	1.0214	2.14	0.1566	−0.033	1.618	0.042	4.171	−1.776	3.160	−20.387	5.230	−9.629
L.OPT-B	(−0.0176, 0.8941, −0.6642, −0.3503, 0.1906, 0.0304)	1	0	0.1569	0.134	1.611	−0.359	4.256	0.217	3.467	−12.850	5.388	−6.889

Note: S = URANS solution of optimal geometry; S_0 = URANS solution of original geometry; Δ = URANS solution difference between optimal and original geometries.
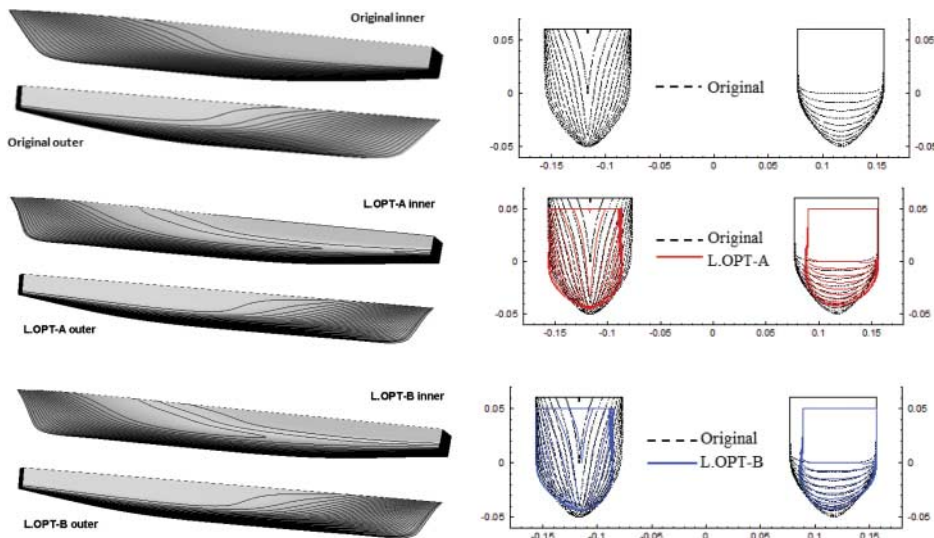

Figure 12.   Optimal design for problem A and B, with comparison with original.

4.4.   *Performance of optimal shapes*

Optimal designs are verified by URANS, as shown in Table 7. Resistance reduction equals 9.63% and 6.89% for L.OPT-A and L.OPT-B, respectively. Displacement variations of final shapes are
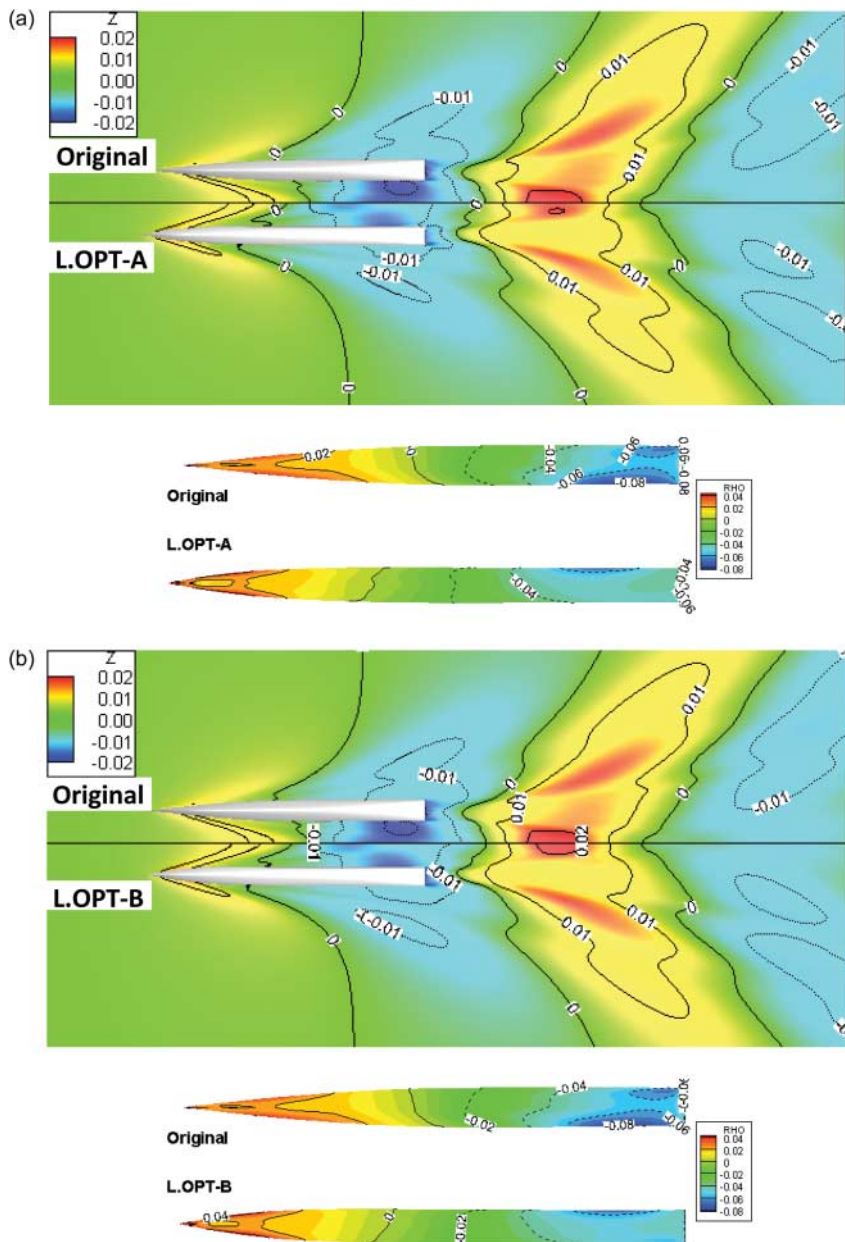
Figure 13. Free surface and pressure distribution for optimal designs, with comparison with original: (a) problem A and (b) problem B.

not significant (−0.17% for L.OPT-A and −0.09% for L.OPT-B). L_{pp} variation for L.OPT-A is 2.14%, corresponding to a 1.05% reduction in the actual Froude number, which equals 0.495.

L.OPT-A and L.OPTB are shown in Figure 12. Compared with the original hull, these slenderize the entire geometry, while moving volume to the bow and the stern (especially at the inner side). The separation distance of the catamaran is increased noticeably. Geometric modifications affect wave elevation and pressure distribution (Figure 13). Wave fields for optimized hulls are smoother than for the original. Elevation variation for the first wave is smaller, as is the divergent component
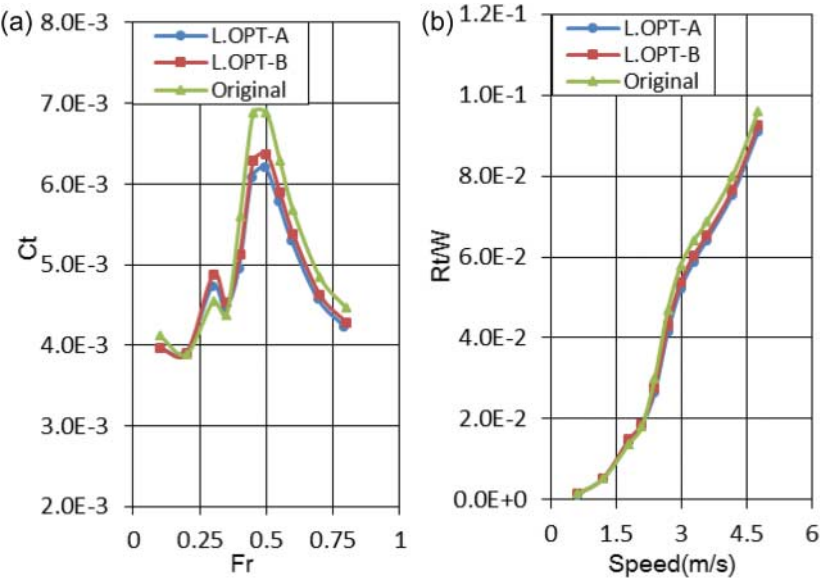
Figure 14.   (a) C_t *vs* Fr; (b) resistance over weight ratio *vs* dimensional speed.
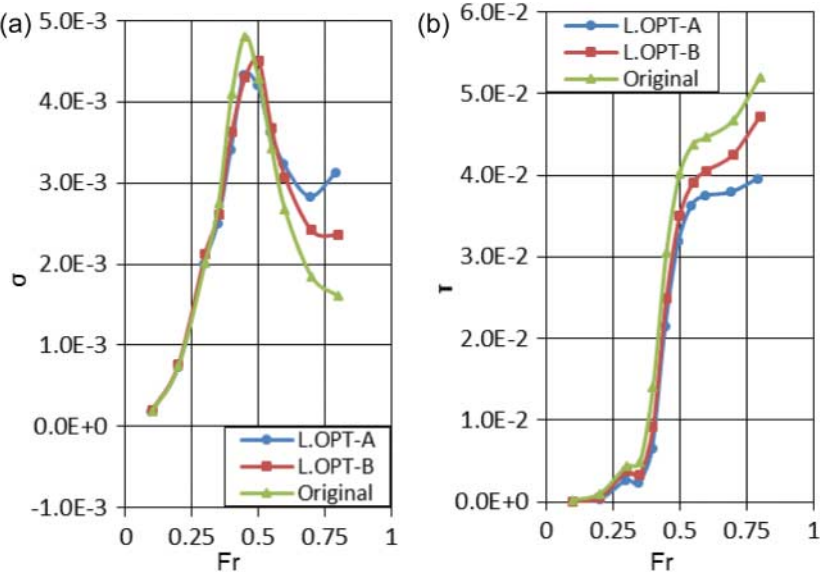

Figure 15.   Non-dimensional sinkage and trim *vs* Fr.

of the disrupted Kelvin wave, reducing the wave resistance. Finally, the negative pressure area on the stern region is smaller than in the original.

A parametric analysis is performed for speed range $0.1 \leq \text{Fr} \leq 0.8$. Non-dimensional (Figures 14a and 15) and dimensional (Figure 14b) results are shown. Optimized hulls show significant improvements in the high-speed range ($0.4 \leq \text{Fr} \leq 0.8$); L.OPT-A is always better than L.OPT-B.

Table 8.   Difference in computational fluid dynamics solutions for L.OPT *vs* original.

Optimum	$\Delta\%S_0$	G1	G2	G3	Aver.
L.OPT-A	R_t/W	−9.953	−9.676	−9.629	−9.753
	σ	−0.654	−1.174	−1.776	−1.202
	τ	−20.478	−20.387	−20.576	−20.480
L.OPT-B	R_t/W	−6.979	−6.792	−6.889	−6.886
	σ	0.669	0.527	0.217	0.471
	τ	−12.837	−12.850	−12.876	−12.854

Table 9.   Verification for L.OPT-A.

L.OPT-A with WJ effect	r	Verification							
		R	P	U_I	U_G	U_I/ε_{12}	$U_I\%U_G$	U_{SN}	$U_{\Delta S}$
C_t	$\sqrt{2}$	0.476	1.072	0.082	2.627	0.079	3.128	2.628	4.550
C_f		0.604	0.728	0.071	1.505	0.132	4.712	1.507	−
C_r		0.443	1.174	0.126	5.428	0.083	2.329	5.429	6.412
σ		0.775	0.368	0.138	10.063	0.101	1.376	10.064	11.017
τ		0.436	1.197	0.016	5.911	0.010	0.271	5.911	6.530

Note: U_I, U_G and U_{SN} are $\%S_1$, where S_1 is the solution of the finest grid.

Table 10.   Verification for L.OPT-B.

L.OPT-B with WJ effect	r	Verification							
		R	P	U_I	U_G	U_I/ε_{12}	$U_I\%U_G$	U_{SN}	$U_{\Delta S}$
C_t	$\sqrt{2}$	0.490	1.029	0.123	2.282	0.108	5.408	2.285	4.361
C_f		0.360	1.472	0.102	1.915	0.281	5.340	1.918	−
C_r		0.524	0.934	0.166	3.371	0.090	4.922	3.375	4.799
σ		0.668	0.582	0.029	3.890	0.030	0.752	3.890	5.934
τ		0.499	1.002	0.017	2.781	0.010	0.598	2.781	3.929

Note: U_I, U_G and U_{SN} are $\%S_1$, where S_1 is the solution of the finest grid. WJ = waterjet.

4.5.   *Verification of optimal shapes*

L.OPT-A and L.OPT-B with WJ model are assessed using one grid triplet with the same size as G1, G2 and G3 in Section 4.1. Table 8 shows that solutions are very close and grid convergent. Table 9 presents the verification of L.OPT-A. U_I is small compared with S_1, ε_{12} and U_G; monotonic convergence is achieved for all variables. P is < 2. U_G is reasonable and has average values for C_t, C_f, C_r, σ and τ equal to 5.11% on the finest grid. Table 10 shows the verification of L.OPT-B. U_I is small compared with S_1, ε_{12} and U_G. Monotonic convergence is achieved for all the variables and P is < 2. U_G is reasonable and gives average values for C_t, C_f, C_r, σ and τ equal to 2.85% on the finest grid. Finally, $U_{\Delta S}$ is equal to 4.5% for L.OPT-A and 4.4% for L.OPT-B, verifying the condition of Equation (16).

5.   Conclusions

Advances in high-fidelity shape optimization have been presented. SBD methodology encompasses geometric variability assessment and design-space dimensionality reduction by KLE, multiple metamodels and multiple deterministic PSO, with the high-fidelity URANS solver. The

application pertained to hull-form design for resistance reduction of the high-speed DC, advancing in calm water at fixed speed and free to sink and trim. Two feasible sets were assessed, considering box constraints (A) and additional constraint on the fixed length between perpendiculars (B).

KLE analysis was performed to reduce the dimensionality of a high-dimensional FFD research space; four dimensions were required to retain 95% of the original geometric variance for set A, whereas six were necessary for set B. Feasible set A was found to have a larger geometric variance than B. Multiple metamodels were trained using a DoE method with high-fidelity URANS simulations and multiple deterministic PSOs were performed. Deterministic PSO was compared to statistically converged stochastic PSO for problem A with the SE-RBFN metamodel, and was confirmed to be effective. Deterministic PSO gave a minimum coincident with that provided by stochastic PSO, using 2% of the computational resources required by the stochastic method. Overall, 120 high-fidelity simulations were used for problem A and 180 for problem B. The final shapes, L.OPT-A and L.OPT-B, achieved a resistance reduction of 9.63% and 6.89%, respectively. Displacement variations were not significant and equalled -0.17% and -0.09% for L.OPT-A and L.OPT-B, respectively. L_{pp} variation for L.OPT-A was 2.14%, corresponding to a 1.05% reduction in actual Froude number, which equalled 0.495. Original and optimal shape simulation uncertainties were studied using verification procedures, revealing $U_{\Delta S}$ equal to 4.5% for L.OPT-A and 4.4% for L.OPT-B. Parametric studies, varying the speed, revealed that L.OPT-A had better performance than the original in a large range ($0.4 \leq \mathrm{Fr} \leq 0.8$) and was always better than L.OPT-B; therefore, L-OPT-A is preferred for future towing tank experiments. Compared with earlier work (Kandasamy *et al.* 2013), the present methodology is deemed more effective and efficient, since it provides an additional improvement of 6.6% for calm-water resistance at 1/10 of the computational cost.

Future developments include fully discretized DC waterjet model design with a focus on inlet and curvature optimization (Chen *et al.* 2013), with validation of the final results by towing tank experiments; and multi-objective optimization of the DC hull in a real operating scenario with stochastic sea state, speed and heading for increased operability and expected reduction in resistance (Diez *et al.* 2013). Future work will also include the development and application of dynamic metamodels (Volpi 2013).

Acknowledgements

Funding

References

Borzì, A., V. Schulz, C. Schillings, and G. Von Winckel. 2010. "On the Treatment of Distributed Uncertainties in PDE-Constrained Optimization." *GAMM-Mitteilungen* 33 (2): 230–246.

Campana, E. F., D. Peri, Y. Tahara, and F. Stern. 2006. "Shape Optimization in Ship Hydrodynamics Using Computational Fluid Dynamics." *Computer Methods in Applied Mechanics and Engineering* 196 (1–3): 634–651.

Campana, E. F., G. Liuzzi, S. Lucidi, D. Peri, V. Piccialli, and A. Pinto. 2009. "New Global Optimization Methods for Ship Design Problems." *Optimization and Engineering* 10: 533–555.

Chen, X., M. Diez, M. Kandasamy, E. F. Campana, and F. Stern. 2013. "Design Optimization of the Waterjet-Propelled Delft Catamaran in Calm Water using URANS, Design of Experiments. Metamodels and Swarm Intelligence." *12th International Conference on Fast Sea Transportation*, FAST2013, Amsterdam, The Netherlands.

Diez, M., E. F. Campana, and F. Stern. 2012. "Karhunen–Loève Expansion for Assessing Stochastic Subspaces in Geometry Optimization and Geometric Uncertainty Quantification." IIHR Technical Report No. 481.

Diez, M., E.F. Campana, and F. Stern. 2013. "Uncertainty Quantification of Delft Catamaran Resistance, Sinkage and Trim for Variable Froude Number and Geometry Using Metamodels, Quadrature and Karhunen–Loève Expansion." *Journal of Marine Science and Technology*, in press. doi:10.1007/s00773-013-0235-0

Diez, M., X. Chen, E. F. Campana and F. Stern. 2013. "Reliability-Based Robust Design Optimization for Ships in Real Ocean Environment." *12th International Conference on Fast Sea Transportation*, FAST2013, Amsterdam, The Netherlands.

Eberhart, R., and Y. Shi. 2000. "Comparing Inertia Weights and Constriction Factors in Particle Swarm Optimization." Evolutionary Computation, 2000. Proceedings of the 2000 Congress on (Volume: 1).

Goel, T., R. Haftka, W. Shyy, and N. Queipo. 2007. "Ensemble of Surrogates." *Structural and Multidisciplinary Optimization* 33 (3): 199–216.

Grigoropoulos, G. J., and D. S. Chalkias. 2010. "Hull-Form Optimization in Calm and Rough Water." *Computer-Aided Design* 42 (11): 977–984.

Haftka, R. T., and R. V. Grandhi. 1986. "Structural Shape Optimization—A Survey." *Computer Methods in Applied Mechanics and Engineering* 57: 91–106.

He, W., M. Diez, Z. Zou, E. F. Campana, and F. Stern. 2013. "URANS Study of Delft Catamaran Total/Added Resistance, Motions and Slamming Loads in Head Sea Including Irregular Wave and Uncertainty Quantification for Variable Regular Wave and Geometry." *Ocean Engineering* 74: 189–217.

Huang, J., P. Carrica, and F. Stern. 2008. "Semi-Coupled Air/Water Immersed Boundary Approach for Curvilinear Dynamic Overset Grids with Application to Ship Hydrodynamics." *International Journal Numerical Methods Fluids* 58: 591–624.

Jakobsson, S., and O. Amoignon. 2007. "Mesh Deformation Using Radial Basis Functions for Gradient-Based Aerodynamic Shape Optimization." *Computers & Fluids* 36 (6): 1119–1136.

Kandasamy, M., Ooi, S. K., Carrica, P., and Stern, F. 2010. "Integral Force/Moment Waterjet Model for CFD Simulations." *Journal of Fluids Engineering* 132 (10): 101–103.

Kandasamy, M., D. Peri, Y. Tahara, W. Wilson, M. Miozzi, S. Georgiev, E. Milanov, E. F. Campana, and F. Stern. 2013. "Simulation Based Design Optimization of Waterjet Propelled Delft Catamaran." *International Shipbuilding Progress*, 60 (1): 277–308.

Kennedy, J., and R. Eberhart. 1995. "Particle Swarm Optimization." *Proceedings IEEE International Conference on Neural Networks*, 1995, 4, 1942–1948.

Kotinis, M., and A. Kulkarni. 2012. "Multi-Objective Shape Optimization of Transonic Airfoil Sections Using Swarm Intelligence and Surrogate Models." *Structural and Multidisciplinary Optimization* 45 (5): 747–758.

Mohammadi, B., and O. Pironneau. 2004. "Shape Optimization in Fluid Mechanics." *Annual Review of Fluid Mechanics* 36: 255–279. doi:10.1146/annurev.fluid.36.050802.121926.

Mousaviraad, S. M., W. He, M. Diez, and F. Stern. 2013. "Framework for Convergence and Validation of Stochastic Uncertainty Quantification and Relationship to Deterministic Verification and Validation." *International Journal of Uncertainty Quantification* 3 (5): 371–395. doi:10.1615/Int.J.UncertaintyQuantification.2012003594.

Papadrakakis, M., Y. Tsompanakis, and N. D. Lagaros. 1999. "Structural Shape Optimization Using Evolution Strategies." *Engineering Optimization* 31 (4): 515–540.

Peri, D. 2009. "Self-Learning Metamodels for Optimization." *Ship Technology Research* 56: 94–108.

Peri, D., and E. F. Campana. 2008. "Variable Fidelity and Surrogate Modeling in Simulation-Based Design." *27th ONR Symposium on Naval Hydrodynamics*, Seoul (Korea).

Peri, D., and F. Tinti. 2012. "A Multistart Gradient-Based Algorithm with Surrogate Model for Global Optimization." *Communications in Applied and Industrial Mathematics* 3 (1): 393 1–22. doi:0.1685/journal.caim.393.

Raghavan, B., P. Breitkopf, Y. Tourbier, and P. Villon. 2013. "Towards a Space Reduction Approach for Efficient Structural Shape Optimization." *Structural and Multidisciplinary Optimization* 48 (5): 987–1000. doi:10.1007/s00158-013-0942-5.

Samareh, J. A. 2001. "Survey of Shape Parameterization Techniques for High-Fidelity Multidisciplinary Shape Optimization." *AIAA Journal* 39 (5): 877–884.

Schillings, C., S. Schmidt, and V. Schulz. 2011. "Efficient Shape Optimization for Certain and Uncertain Aerodynamic Design." *Computers & Fluids* 46 (1): 78–87.

Shi, Y., and R. Eberhart. 1998. "A Modified Particle Swarm Optimizer." *Evolutionary Computation Proceedings*, 1998. IEEE World Congress on Computational Intelligence.

Suykens, J. A. K., T. V. Gestel, J. D. Brabanter, B. D. Moor, and J. Vandewalle. 2002. *Least Squares Support Vector Machines*. Singapore: World Scientific.

Tahara, Y., D. Peri, E. F. Campana, and F. Stern. 2011. "Single- and Multiobjective Design Optimization of a Fast Multihull Ship: Numerical and Experimental Results." *Journal of Marine Science and Technology* 16: 412–433.

Volpi, S. 2013. "Development of Dynamic Metamodels for Design Optimization and Uncertainty Quantification." Master's thesis dissertation, University of Rome Tre, Rome, Italy, October.

Wahba, G. 1990. *Spline Models for Observational Data*. Philadelphia: Society for Industrial and Applied Mathematics.

Won, K. S., and T. Ray. 2005. "A Framework for Design Optimization using Surrogates." *Engineering Optimization* 37 (7): 685–703.

Wong, T.-T., W.-S. Luk, and P. A. Heng. 1997. "Sampling with Hammersley and Halton Points." *Journal of Graphics Tools* 2 (2): 9–24.

Xing, T., and F. Stern. 2010. "Factors of Safety for Richardson Extrapolation." *Journal of Fluids Engineering* 132 (6): 061403 1–13.

Zhao, L., K. Choi, and I. Lee. 2011. "Metamodeling Method using Dynamic Kriging for Design Optimization." *AIAA Journal* 49 (9): 2034–2046.